Nanoscale

Accepted Manuscript

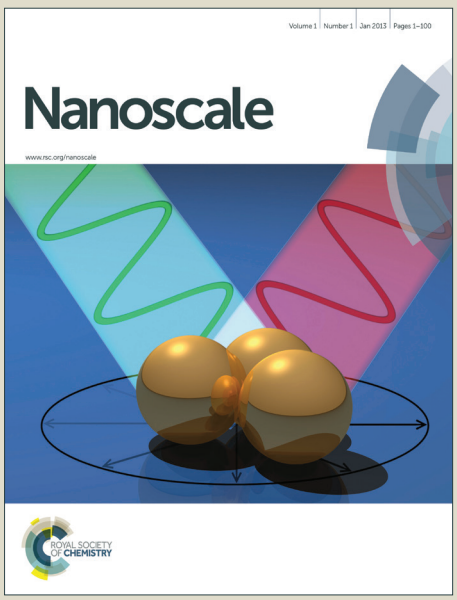

ROYAL SOCIETY OF CHEMISTRY

www.rsc.org/nanoscale

Amine-modified Hyaluronic Acid-functionalized Porous Silicon Nanoparticles for Breast Cancer Targeting

Patrick V. Almeida[a], *Mohammad-Ali Shahbazi*[a], *Ermei Mäkilä*[a,b], *Martti Kaasalainen*[b], *Jarno Salonen*[b], *Jouni Hirvonen*[a], *Hélder A. Santos**[a]

[a] *Division of Pharmaceutical Chemistry and Technology, Faculty of Pharmacy, FI-00014 University of Helsinki, Finland*

[b] *Laboratory of Industrial Physics, Department of Physics and Astronomy, FI-20014 University of Turku, Finland*

***Address correspondence:**

helder.santos@helsinki.fi

Tel.: +358 2941 59661

Fax.: +358 2941 59138

TABLE OF CONTENTS GRAPHICAL ABSTRACT

Synthesis of amine-modified hyaluronic acid-porous silicon nanoparticles result in a suitable and promising nanodelivery system for targeting of CD44-overexpressing cell tumors.

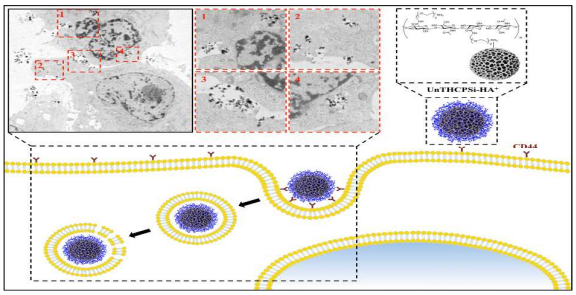

ABSTRACT

Active targeting of nanoparticles to receptors overexpressing cancer cells has great potential for enhancing nanoparticle cell uptake and for reducing fast clearance of the nanoparticles from the body. Herein, we present the preparation method of porous silicon (PSi)-based nanodelivery system for breast cancer targeting, by covalently conjugating a synthesized amide-modified hyaluronic acid (HA^+) derived polymer on the surface of undecylenic acid-modified thermally hydrocarbonized PSi (UnTHCPSi) nanoparticles. The resulting UnTHCPSi–HA^+ nanoparticles showed relatively small size, reduced polydispersibility, high biocompatibility, improved colloidal and human plasma stability, as well as enhanced cellular interactions and internalization. Moreover, we demonstrated that the enhanced cellular association of UnTHCPSi–HA^+ relies on the capability of the conjugated HA^+ to bind and consequently target CD44 receptor expressed on the surface of the breast cancer cells, thus making the HA^+-functionalized UnTHCPSi nanoparticles a suitable and promising nanoplatform for targeting of CD44 overexpressing breast tumors and for drug delivery.

Keywords: Porous silicon nanoparticles; Amine-modified hyaluronic acid; Surface functionalization; CD44 receptor targeting; Breast cancer

† **Electronic supplementary information (ESI) available.** See DOI: 10.1039/XXXXX

Introduction

Cancer is a complex disease estimated to have caused more than 8.2 million deaths, counted with approximately 14.1 million new cases in 2012, and forecasted to reach over 25 million new cases in the next two decades, representing one of the leading causes of death worldwide. [1]

Although the 21st century has seen remarkable strides in fundamental cancer biology and genetics, the advances have not always been translated into comparable clinical success stories. In fact, a large number of nanoparticulate drug delivery systems suffer from easy recognition by the reticuloendothelial system (RES), poor targeting efficiency, and consequent rapid elimination by the liver and spleen, hindering the effective release of the loaded therapeutic cargo(s) at the tumor site due to insufficient blood circulation time and non-specific tissue distribution. [2]

After intravenous administration, the *in vivo* fate of nanoparticles is significantly influenced by the interactions between particles and plasma proteins, possibly resulting in protein adsorption on the nanoparticles surface, protein corona formation and undesirable opsonization by the RES. [3-6] In addition to the acknowledged passive accumulation of the nanoparticles in the tumor sites by the enhanced permeation and retention effect (EPR), [7, 8] the intracellular localization of the therapeutic target of most anticancer agents requires the design and development of targeting nanocarriers capable of being actively accumulated at the tumor site, being internalized by the cancer cells, and ultimately release its payloads intracellularly. Therefore, there is an imperative demand for engineering new targeting nanodelivery systems possessing improved stability in human plasma and capability of efficiently and safely delivering the therapeutic agents to the targeted tumor tissues. [9, 10]

Mesoporous materials, particularly porous silicon (PSi), have recently emerged as a promising platform for drug delivery [11-15] and imaging [11, 15, 16] applications. PSi is a material

traversed by nanoscale pores in a crystalline Si structure, encompassing several attractive physical properties, such as top-down manufacturing method, [11, 12, 17] fine-tunable nanoscale sizes, high surface-to-volume ratio, as well as large surface area and pore volume. [11, 12, 14] The PSi mesoporous structure has been proved to enable the efficient loading of multiple therapeutic agents within its pores, including poorly-water soluble drugs, [12, 18-23] peptides, [24-26] and siRNA, [27, 28] with optimized and reproducible dissolution and release profiles. Additionally, PSi is characterized by suitable biocompatibility, [18, 19, 29-31] biodegradability in non-toxic products, [15, 30-32] and easy surface modification. [12, 33]

A variety of chemical treatments of the PSi's surface are well established, with emphasis on thermal oxidation (TOPSi) and hydrocarbonization (THCPSi), rendering the PSi materials hydrophilic or hydrophobic properties, respectively. [12, 25] Moreover, a variety of active groups, including amine, [21, 34, 35] carboxylic, and alkyne, [36] can be grafted on the PSi nanoparticles surface and subsequently functionalized with different bioactive moieties, aiming at the modulation of plasma protein adsorption, [35, 37]adaptation to gastrointestinal environment, [38-40]improvement of tumor-targeting efficiency, [41, 42]and/or enhancement of cellular association and internalization. [35, 39]

Recently, hyaluronic acid (HA), a linear glycosaminoglycan consisting of alternating D-glucoronic acid and N-acetyl-D-glucosamine units, has been highlighted as a tumor targeting moiety, relied on its major affinity to CD44 receptor, a type 1 transmembrane glycoprotein up-regulated in a large variety of cancer cells. [43, 44] Furthermore, CD44 is known to play a key role in a wide diversity of biological processes, including cell proliferation, differentiation and migration, as well as in angiogenesis, tumor invasion, and metastasis. [45-48] Although involved in diverse physiological and pathological processes, therefore being expressed in non-malignant tissues, [49, 50] the CD44 receptor has been shown to be over-expressed in tumor tissues, and a correlation between such occurrence *vs.* tumor genesis and metastasis *in vivo*

has already been established. [51, 52] In addition to its biological functions, HA presents interesting physicochemical properties, such as high water-solubility, biocompatibility, biodegradability, non-immunogenicity, and chemical structure suitable for further functionalization, which all together make this versatile polymer an attractive biomaterial to be applied concomitantly as a targeting and stabilizing moiety in the development of cancer targeting drug delivery systems. [53, 54]

Herein, we have developed a nanosystem based on the surface biofunctionalization of undecylenic acid-functionalized thermally hydrocarbonized PSi (UnTHCPSi) nanoparticles with an amine-modified hyaluronic acid derivative, aiming both to increase the targeting efficiency of the PSi nanoplatform and also to overcome some of its limitations, such as the colloidal stability and plasma protein adsorption. Particularly, we aimed to combine the specific targeting affinity of HA for CD44-overexpressing cancer cells with the distinctive physicochemical and biological properties of the PSi nanoparticles into a single nanocarrier, moving towards the circumvention of the deadlocks associated with the currently available nanomedicines, particularly in the field of cancer targeting and therapy.

Experimental

Materials and reagents

The materials and reagents used in all the experiments performed in this study can be found in the Supplementary data.

Fabrication of UnTHCPSi nanoparticles

The fabrication of the PSi nanoparticles was done using electrochemical anodization, previously described in detail elsewhere. [18, 26] Briefly, monocrystalline boron-doped p+-type Si ⟨100⟩ wafers, with a resistivity of 0.01–0.02 Ω.cm, were electrochemically anodized in a

1:1 (v/v) aqueous hydrofluoric acid (40%)-ethanol electrolyte, by applying an etching profile consisting of consecutive low and high current density pulses. The resulting PSi with hydrogen-terminated surface was subsequently detached from the substrate as free-standing multilayer films by increasing the current density to the electropolishing region. The films were then dried and introduced in a quartz tube under N_2-flow (1 L/min) for at least 30 min at room temperature, in order to remove residual oxygen and adsorbed moisture. Thermal hydrocarbonization of the PSi films was performed by exposure to a 1:1 (v/v) N_2/acetylene (C_2H_2)-flow (1 L/min) for 15 min at room temperature, followed by a heat treatment for 15 min at 500 ºC, in order to produce a hydrocarbon termination. The obtained THCPSi films were then treated in 10-undecenoic acid for 16 h at 120 ºC. The UnTHCPSi films were finally wet-milled to produce nanoparticles. The final size selection of the PSi nanoparticles was done using centrifugation.

Synthesis of amine-modified hyaluronic acid (HA^+)

The method used for the synthesis of amine-modified hyaluronic acid (HA^+) was previously described elsewhere. [55]An aqueous solution of HA sodium salt (200 mg, 30 mmol) was dialyzed against 0.01 N HCl (4 L) for 20 h, followed by a dialysis against Milli-Q water (4 L) for 20 h. The resulting acidic form of HA (172 mg, 0.45 mmol of acidic groups) was recovered by lyophilization, and subsequently dissolved in 14 mL of anhydrous DMSO, together with 80 mg (0.70 mmol) of N-hydroxysulfosuccinimide (NHS). Afterwards, 124 µL (109 mg, 0.70 mmol) of 1-ethyl-3-[3-dimethylaminopropyl]carbodiimide (EDC) (≥97.0%) was added to the solution, under stirring, and the activation of the carboxylic groups of HA was allowed to proceed for 60 min at room temperature, in the dark. The substitution of the carboxylic groups of HA was carried out by adding NH_2-PEG_2-NHBoc (223 mg, 0.90 mmol, 2 eq) and N-ethyldiisopropylamine (DIPA) (70 mg, 0.54 mmol, 1.2 eq), under stirring. The

reaction was allowed to proceed for 4 days. After completion of the reaction, the resulting HA-PEG_2-NHBoc was precipitated in acetone (140 mL), washed three times with acetone (3× 100 mL), and then filtered and dried under vacuum to remove the residues of DMSO. The deprotection of the terminal amine of HA-PEG_2-NHBoc was performed by dissolving 50 mg of the polymer in 5 mL of trifluoroacetic acid (TFA) at 0 ºC, and the solution was left under stirring at 4 ºC for 20 h. After this time, 20 mL of Milli-Q water was added, and the solution was neutralized using NaOH. The sodium salt of the HA^+ was obtained by dialyzing the solution against 0.1 M NaCl (2 L) for 20 h and afterwards against Milli-Q water (2 L) for the same time. The final HA^+ sodium salt was recovered by lyophilization and the corresponding Fourier transform infrared spectroscopy (FTIR) spectrum was obtained and analyzed against the spectra of the starting materials.

Preparation of UnTHCPSi–HA^+ nanoparticles

The UnTHCPSi–HA^+ nanoparticles were prepared by covalently conjugating the synthesized amine-terminated HA^+ to the carboxylic groups of UnTHCPSi nanoparticles, via EDC/NHS coupling chemistry in an aqueous environment. This polymeric functionalization was performed by dispersing 1.5 mg of the UnTHCPSi nanoparticles in 4 mL of 10 mM 2-(*N*-morpholino)ethanesulfonic acid (MES) saline buffer at pH 5.2. For activating the precursor carboxylic groups of the UnTHCPSi nanoparticles, 6 mg (0.05 mmol) of NHS and 8 μL (0.05 mmol) of EDC (≥97.0%) were added to the UnTHCPSi nanoparticles suspension, after which the reaction was stirred at 800 rpm for 90 min, in the dark. The surface activated UnTHCPSi were then exposed to free amine-terminated HA^+ at a w/w ratio of 2:1 (HA^+:UnTHCPSi nanoparticles), and the nucleophilic substitution was allowed to proceed overnight in the same stirring conditions. The excess of the starting reagents, including EDC, NHS, and unconjugated HA^+ were removed by rinsing the resulting UnTHCPSi–HA^+ nanoparticles

three times with Milli-Q water. Finally, the UnTHCPSi–HA^+ nanoparticles were re-dispersed in Hank's balanced salt solution–4-(2-hydroxyethyl)-1-piperazineethanesulfonic acid (HBSS–HEPES) buffer at pH 7.4, and stored at 4 ºC until further use.

Physicochemical characterization of UnTHCPSi and UnTHCPSi–HA^+

The surface chemical characterization of UnTHCPSi and UnTHCPSi–HA^+ nanoparticles was performed by analyzing the FTIR spectra of the samples using a Bruker VERTEX 70 spectrometer (Bruker Optics Inc., USA) fitted with a horizontal attenuated total reflectance (ATR) accessory (MIRacle PIKE Technologies, USA) and a Mattson Galaxy 6020 spectrometer (Mattson Instruments, USA) equipped with a PA301 photoacoustic detector (Gasera Ltd., Finland) using He as the carrier gas. The absorbance spectra were recorded in the wavenumber region between 4000 and 650 cm^{-1} with a 4 cm^{-1} resolution. All the samples were dried at room temperature for 48 h prior to the FTIR measurements.

The physical properties of bare UnTHCPSi, namely the specific surface area, total pore volume, and average pore diameter, were determined by N_2-sorption at −196ºC, using a TriStar 3000 equipment (Micromeritics Inc., USA). The specific surface area was calculated using the Brunauer-Emmett-Teller (BET) theory. [56] The total pore volume was considered to be the total adsorbed amount at a relative pressure p/p_0=0.97. [57] The average pore diameter was calculated from the values of specific surface area and total pore volume, assuming the pores of the UnTHCPSi nanoparticles as cylindrical.

Particle size was measured from dynamic light scattering (DLS). The average hydrodynamic particle size (Z-average) and polydispersity index (PdI) were calculated with cumulants algorithm and particle size distributions were obtained from the distribution fit of Zetasizer Nano ZS equipment (Malvern Instruments Ltd, UK). Also, the zeta (ζ)-potential measurements were made using the aforementioned equipment utilizing its electrophoretic

light scattering (ELS) setup. Prior to the measurements, each of the samples were centrifuged and re-dispersed in Milli-Q water at a final concentration of 25 μg/mL. All the sample measurements were performed in triplicate.

The size and morphology of UnTHCPSi and UnTHCPSi–HA^+ nanoparticles were analyzed by transmission electron microscope (TEM). The TEM pictures were captured using a Jeol JEM-1400 microscope (Jeol Ltd., Tokyo, Japan) with an 80 kV voltage. The nanoparticle suspensions were centrifuged, re-dispersed in ethanol at a concentration of 10 μg/mL, and dropped in a carbon-coated copper TEM grid, followed by drying for 48 h at room temperature.

Stability studies in human plasma

For performing these experimens, 300 μg of UnTHCPSi and UnTHCPSi–HA^+ were dispersed in 200 μL of 1× PBS (pH 7.4), exposed to 1500 μL of human plasma, and left under stirring at 800 rpm and 37 ºC for 2 h. Sampling aliquots of 200 μL were withdrawn at pre-determined time points (1, 5, 10, 15, 30, 60, 90, and 120 min), and the correspondent size, ζ-potential, and PdI were subsequently determined by DLS and ELS. The results are shown as the average of at least three independent measurements. Anonymous human plasma donors were obtained from the Finnish Red Cross Blood Service, under the permission from the respective institutional ethical committee.

Cell lines and culturing conditions

For the *in vitro* studies, MCF-7 and MDA-MB-231 breast cancer cells were cultured according to the protocols described in detail in the Supplementary Data.

In vitro cytotoxicity studies

The *in vitro* cytotoxicity of both UnTHCPSi and UnTHCPSi–HA^+ was evaluated by a CellTiter-Glo® Luminescent Cell Viability assay, as previously described elsewhere. [26, 29] MCF-7 and MDA-MB-231 breast cancer cells were suspended in the correspondent cell culturing media at a concentration of 2×10^5 cells/mL, and approximately 2×10^4 cells/well were seeded in 96-well plates (Corning Inc. Life Sciences, USA). The cells were allowed to attach overnight at 37 ºC, after which the cell culturing media was removed and replaced with 100 µL of UnTHCPSi and UnTHCPSi–HA^+ nanoparticles suspensions at concentrations of 25, 50, and 100 µg/mL, as well as with 1× HBSS (pH 7.4) and 1% Triton X-100, assumed as positive and negative controls, respectively. After incubation for 6 and 24 h at 37 ºC, 100 µL of the assay reagent was added to each well and the number of viable cells was determined by measuring the luminescence of the wells using a Varioskan Flash fluorometer (Thermo Fisher Scientific Inc., USA). The results presented correspond to the average of at least three independent measurements.

Cellular internalization

The cellular uptake and intracellular localization of the UnTHCPSi and UnTHCPSi–HA^+ nanoparticles was assessed by TEM. Approximately 10^5 cells/well of MCF-7 and MDA-MB-231 breast cancer cells were seeded in 24-well plates (Corning Inc. Life Sciences, USA) containing 13 mm round shaped coverslips and allowed to attach overnight at 37 ºC. After removing the cell culture media, 500 µL/well of the nanoparticle suspensions at concentration of 50 µg/mL were added to the wells. After an incubation period of 6 h at 37 ºC, the nanoparticle suspensions were carefully removed and the samples were rinsed twice with HBSS–HEPES (pH 7.4). The cells were fixed with 2.5% glutaraldehyde in 0.1 M PBS

buffer (pH 7.4) for 1 h at room temperature, and subsequently washed twice with HBSS–HEPES (pH 7.4) and with sodium cacodylate buffer (NaCac) for 3 min, prior post-fixation with 1% osmium tetroxide in 0.1 M NaCac buffer (pH 7.4). Thereafter, the cells were dehydrated with 30–100% ethanol for 10 min and embedded in epoxy resin. Ultrathin sections with approximately 60 nm were sliced parallel to the coverslips, post-stained with uranyl acetate and lead citrate, and finally analyzed by TEM as described above.

Flow cytometric analysis of CD44 expression and cellular association

The expression of CD44 receptor in MCF-7 and MDA-MB-231 breast cancer cell lines was evaluated by flow cytometry according to a protocol adapted from the manufacturer's instructions, as described in the Supplementary Data.

Flow cytometric analysis was also performed to evaluate the cellular association of UnTHCPSi and UnTHCPSi–HA^+ nanoparticles. The nanoparticles were primarily labeled with fluorescein isothiocyanate (FITC). For that purpose, FITC was dissolved in a 1:5 (v/v) ratio of 0.1 M HEPES (pH 7.5) and ethanol. The labeling of the nanoparticles was achieved by adding the FITC solution to the nanoparticles in a 10:1 ratio. MCF-7 and MDA-MB-231 breast cancer cells were seeded in 6-well plates at a density of 7×10^5 cells/well and allowed to attach overnight at 37 ºC. The attached cells were subsequently washed with HBSS–HEPES (pH 7.4) and exposed to the FITC-labeled nanoparticles at the concentrations of 50 and 100 μg/mL for 6 h at 37 ºC. The cells were then harvested using 300 μL of 0.25% trypsin-PBS-EDTA solution and washed three times with HBSS–HEPES (pH 7.4), after centrifugation at 500 rpm for 3 min in order to remove the non-associated nanoparticles. Prior to the flow cytometric analysis, the cells were fixed with 2.5% glutaraldehyde in 0.1 M PBS buffer (pH 7.4) for 30 min and re-suspended in 700 μL of HBSS–HEPES (pH 7.4). The measurements were performed using a LSR II flow cytometer (BD Biosciences, USA), with

the laser excitation wavelength of 488 nm. A minimum of 10000 events per sample were collected using FACSDiva software. The data was analyzed and plotted using Flowjo 7.6 software (Tree Star, Ashland, USA).

Statistical analysis

Results are expressed as the mean ± s.d. of at least three independent measurements. The results obtained in the aforementioned experiments were statistically analyzed by means of the Student's *t*-test with the level of significance set at probabilities of $*p < 0.05$, $**p < 0.01$, and $***p < 0.001$. The analysis was performed using GraphPad Prism 5 software (GraphPad Software Inc., USA).

Results and discussion

Preparation and characterization of the nanoparticles

Active targeting of nanoparticles to receptors overexpressing cancer cells has great potential for enhancing both the nanoparticle cell uptake and for reducing the fast clearance of the nanoparticles from the body.[2] Therefore, in order to evaluate the potential of PSi-based materials to specifically target the CD44 receptor overexpressed in breast cancer cells, an amine-modified hyaluronic acid (HA^+) was synthesized and subsequently used to functionalize the surface of bare UnTHCPSi nanoparticles to form UnTHCPSi–HA^+ nanoparticles. The UnTHCPSi nanoparticles were prepared by electrochemical anodization as previously described elsewhere, [18, 26] and according to the procedure depicted in Scheme 1A. Moreover, the amine-modified hyaluronic acid (HA^+) was synthesized by a carbodiimide-mediated coupling of the NH_2-PEG_2-NHBoc polymer to the carboxylic groups of HA in DMSO. [55] Briefly, active esters of HA were formed with NHS using EDC as a coupling agent. The nucleophilic addition of the mono-protected di-amine to the HA ester

requires it to be in an unprotonated form, which can be achieved in the presence of DIPA. After coupling, the free amine can be obtained by deprotection using TFA. The further covalent conjugation of HA^+ onto the surface of the UnTHCPSi nanoparticles was performed in aqueous solution by using EDC/NHS chemistry. For this polymeric functionalization, the carboxyl groups of the UnTHCPSi nanoparticles were activated, working as precursors for the subsequent covalent attachment of HA^+ through its free amine groups. The hypothesis for the targeted therapy of CD44-overexpressing breast cancer cells of the developed nanoparticles is depicted in Scheme 1B.

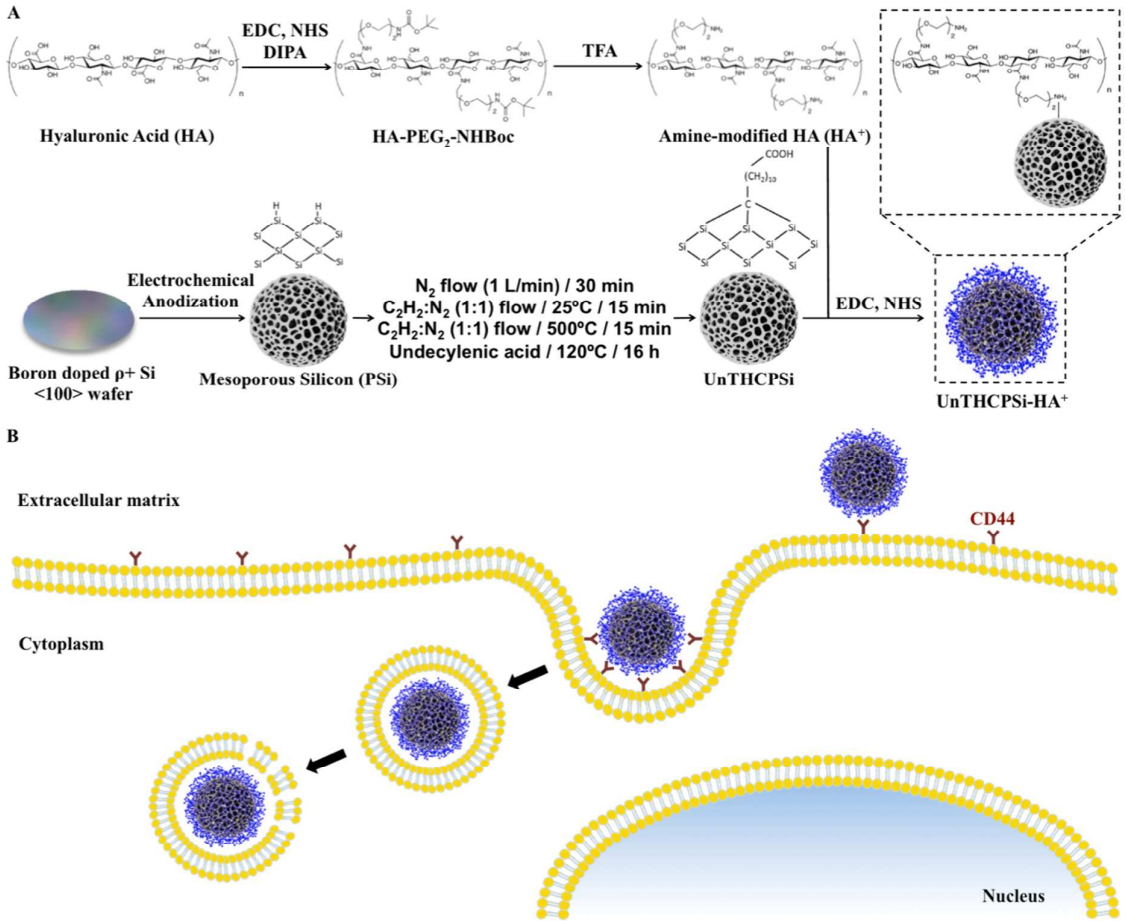

Scheme 1. (A) Schematic illustration of the synthesis of HA^+, fabrication of UnTHCPSi nanoparticles from boron doped p+ Si ⟨100⟩ wafer, conjugation of HA^+ onto the surface of the UnTHCPSi nanoparticles via EDC/NHS coupling chemistry. **(B)** Hypothesis of the

application of the resulting UnTHCPSi–HA^+ for targeting of CD44-overexpressing breast cancer cells.

The TEM images of both UnTHCPSi and UnTHCPSi–HA^+ nanoparticles are presented in Figure 1A. Furthermore, the colloidal stability of UnTHCPSi and UnTHCPSi-HA^+ in HEPES buffer (pH 7.4) was evaluated by comparing the visual appearance of both the nanoparticles dispersions in HBSS–HEPES (pH 7.4), after storage at room temperature for 4 h (Figure 1B). It was observed that the UnTHCPSi–HA^+ nanoparticles were considerably more stable in the referred ionic aqueous environment when compared with their bare counterparts, which evidenced aggregation and precipitation phenomena over time due to their surface properties. The increased stability of UnTHCPSi–HA^+ nanoparticles can be explained by the steric stabilization phenomenon resulting from conjugation of HA^+ onto the surface of UnTHCPSi nanoparticles.

The UnTHCPSi nanoparticles used in the present work presented a specific surface area of 218 ± 3 m^2/g, a total pore volume of 0.63 ± 0.01 cm^3/g, and an average pore diameter of 12.2 ± 0.4 nm. In addition, the mean particle size, PdI, and ζ-potential of the UnTHCPSi and UnTHCPSi–HA^+ nanoparticles were determined by DLS (ESI S1†). The *Z*-average diameter of the UnTHCPSi and UnTHCPSi–HA^+ nanoparticles was 208.1 ± 1.6 nm and 228.3 ± 2.6 nm, with a PdI of 0.07 ± 0.01 and 0.09 ± 0.02, respectively, demonstrating an expected increase on the size of UnTHCPSi after the conjugation of HA^+ (Supporting Data, Figure S1A). The PdI, which is an indicator of the particle size distribution, was found to be less than 0.1 in both samples (Supporting Data, Figure S1B), demonstrating the high monodispersibility of the prepared nanoparticle suspensions. The presence of carboxylic groups on the surface of UnTHCPSi rendered its surface strongly negatively charged, presenting a measured ζ-potential of –41.6 ± 1.5 mV. After the polymeric functionalization

with HA^+, the ζ-potential turned slightly less negative (–17.7 ± 0.4 mV), possibly due to the presence of free amines from HA^+ on the surface of UnTHCPSi–HA^+ (Supporting Data, Figure S1C). These results indicated the successful polymer conjugation of HA^+ onto the surface of the UnTHCPSi nanoparticles.

The FTIR spectra of HA, HA^+, UnTHCPSi and UnTHCPSi-HA^+ nanoparticles are presented in Figure 1C. The carbohydrate chain of HA can be identified through the prominent C−O band at 900–1200 cm^{-1}, which is characteristic of polysaccharides. Other observable features of HA are the stretching bands at 1607 cm^{-1} (Figure 1C-a2) and 1400 cm^{-1} (Figure 1C-a4), related to the carboxylate C=O and C−O stretching vibrations, respectively. The amide I and II related bands on the other hand, are visible at ca. 1670 cm^{-1} (Figure 1C-a1) and 1540 cm^{-1} (Figure 1C-a3), respectively. [58, 59] The effects of the amine modification for the HA^+ have only limited visible effects on spectra (Figure 1C-b). The basic chemical structure of HA is preserved in the modification, however the appearance of a broad band at ca. 1680 cm^{-1} (Figure 1C-b1) and a peak at 1555 cm^{-1} (Figure 1C-b2) indicate the presence of the amide conjugated NH_2-PEG_2-NHBoc in the polymer. The spectra of the UnTHCPSi nanoparticles (Figure 1C-d) exhibit a broad band between 900−1200 cm^{-1} and a C=O stretching at 1715 cm^{-1} (Figure 1C-d1), corresponding to the Si−C and carboxylic acid group structures, respectively. After functionalization of the UnTHCPSi nanoparticles surface with HA^+ polymer (Figure 1C-c), and comparing to the bare UnTHCPSi spectrum, a broad absorption band corresponding to amide (I) structure arises at 1640 cm^{-1} (Figure 1C-c1) and the amide (II) structure of HA^+ can be recognized at 1555 cm^{-1}, suggesting the successful covalent attachment of the polymer. The described analysis indicated that the HA^+ polymer was successfully synthesized by EDC/NHS reaction and conjugated onto the surface on the UnTHCPSi nanoparticles *via* the same carbodiimide-mediated coupling chemistry.

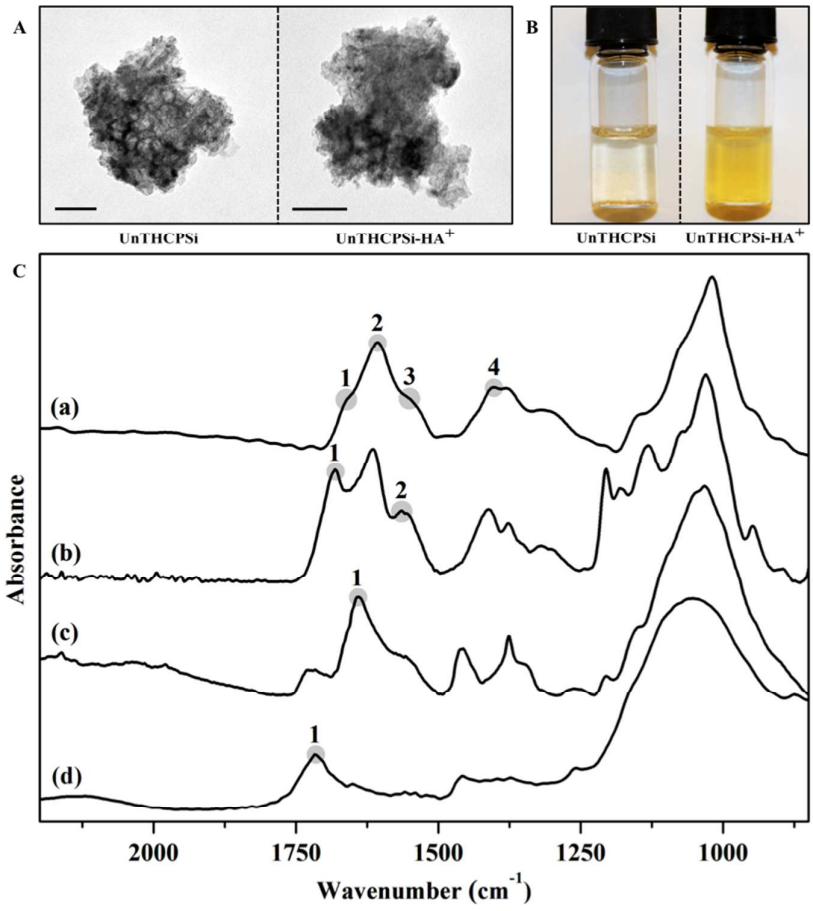

Figure 1. (A) TEM images of the UnTHCPSi and UnTHCPSi–HA^+ nanoparticles. Scale bars are 100 nm. **(B)** Colloidal stability of UnTHCPSi and UnTHCPSi–HA^+ after incubation in HEPES buffer (pH 7.4) at room temperature for 4 h. **(C)** FTIR absorbance spectra of HA **(a)**, HA^+ **(b)**, UnTHCPSi-HA^+ **(c)**, and UnTHCPSi **(d)**. The relevant features each spectrum are highlighted and numbered for clarity (see text for details).

Stability in human plasma

When an intravenous administration is envisioned, the interaction of the plasma proteins with a nanoparticulate system may influence its biofate.

Additionally to the physicochemical characterization of the developed UnTHCPSi–HA^+ nanoparticles, it is essential to understand the nanoparticle–protein interactions, since the

stability in plasma may influence the biofate of the nanoparticles, thus being a major prerequisite for a medical nanodelivery system intended to be administered intravenously. [41] Ideally, nanoparticles injected systemically, should minimally interact with plasma proteins, in order to avoid the rapid opsonization by the RES. The conjugation of polymeric moieties on nanoparticles' surface constitutes one possible strategy to overcome this problem. [60, 61] In this sense, we have investigated the influence of the surface functionalization of the UnTHCPSi–HA^+ nanoparticles on the plasma protein adsorption, by incubating both nanoparticles in human plasma at 37 ºC for 2 h, and subsequently evaluating the effect of such conditions on the *Z*-average, ζ-potential, and PdI of the nanoparticles (Figure 2). Contrarily to the bare UnTHCPSi nanoparticles, where the size increased from an average of ca. 200 nm to ca. 600 nm immediately (after 10 min) in contact with human plasma, no differences in particle sizes were observed for UnTHCPSi–HA^+ throughout the whole 2 h incubation period (Figure 2A). Furthermore, the ζ-potential of the UnTHCPSi nanoparticles was immediately increased from ca. –42 mV to –15 mV, suggesting the expected adsorption of plasma proteins. After the conjugation of HA^+, the ζ-potential remained constant within the 2 h of the experiment. The PdI of both coated and uncoated UnTHCPSi nanoparticles increased when in contact with human plasma (Figure 2C). However, such effect was considerably less significant in the case of UnTHCPSi–HA^+, stabilizing at a constant value of approximately 0.2, suggesting the relative monodispersibility of the nanoparticles suspension. Therefore, when incubated with human plasma, bare UnTHCPSi nanoparticles revealed to be unstable, contrarily to the UnTHCPSi–HA^+ nanoparticles, which exhibited smaller variation in particle size, ζ-potential, and PdI than the UnTHCPSi nanoparticles. Therefore, when conjugated to the nanoparticles' surface, HA^+ may effectively minimize particle aggregation and protein adsorption, resulting in an improved stability of the UnTHCPSi-HA^+ in human plasma. This effect might be explained by the high hydrophilic nature of HA^+, enhancing the

hydrophilicity of the UnTHCPSi nanoparticles' surface. When administered intravenously, the improved plasmatic stability of UnTHCPSi-HA$^+$ nanoparticles is expected to significantly minimize the opsonization by the reticuloendothelial system and, consequently, to increase the blood circulation time of the nanocarrier, as well as its accumulation in the targeted tumor. [62-65]

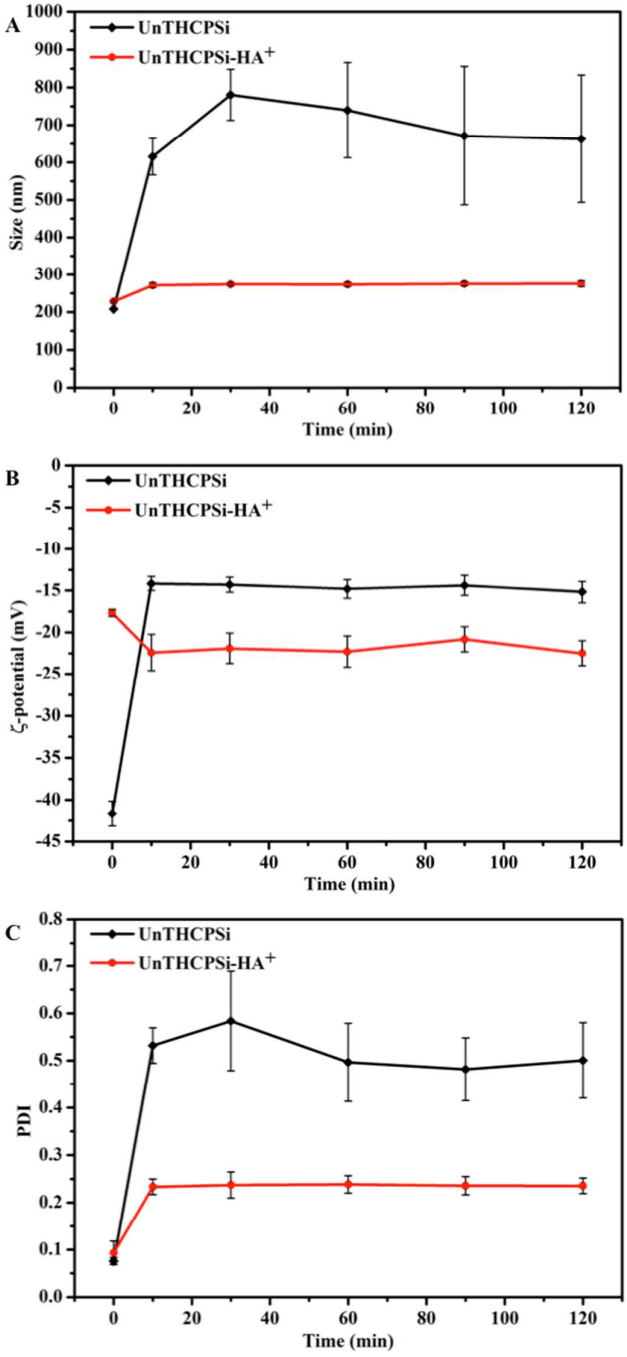

Figure 2. Effect of the human plasma protein adsorption on the size **(A)**, ζ-potential **(B)**, and PDI **(C)**, of the UnTHCPSi and UnTHCPSi–HA^+ nanoparticles after an incubation with human plasma for 120 min at 37 ºC. The results were calculated from the DLS measurements data as a function of time. Values represent the mean ± s.d. ($n \geq 3$).

In vitro cytotoxicity studies

Prior to testing the UnTHCPSi and UnTHCPSi–HA^+ nanoparticles in an *in vitro* setting, their cytocompatibility should be extensively evaluated, in order to determine the range of safe concentrations for further experiments. Therefore, we assessed the cell viability of both MDA-MB-231 and MCF-7 breast cancer cells, following incubation with different concentrations of UnTHCPSi and UnTHCPSi–HA^+ for 6 and 24 h at 37 ºC, by performing an ATP activity-based CellTiter Glo® Luminescence assay (Figure 3). [26, 29] Overall, the results showed no significant cytotoxicity by UnTHCPSi or UnTHCPSi–HA^+ nanoparticles. However, the incubation of MDA-MB-231 cells at 100 μg/mL concentration of both UnTHCPSi and UnTHCPSi–HA^+ nanoparticles for 24 h, resulted in a statistically significant decrease of the cell viability to 72.0 ± 1.9 and 55.8 ± 3.1 %, respectively. The cytotoxic effect observed in these testing conditions might be relate with the increased cellular uptake of the nanoparticles, which might lead to the disruption of the cellular membrane and, consequently, to the depletion of ATP. [18, 29] Furthermore, the internalized nanoparticles might interact with the intracellular mitochondria and compromise its integrity, leading to reduced mitochondrial membrane potential and, subsequently, increased permeability. This, in turn, compromises the state of the mitochondria and impedes the normal electron transport chain, which results in decreased ATP production and cell death. [29, 66] In the case of UnTHCPSi–HA^+ nanoparticles, the remarkably low cytotoxicity values can be explained by the low toxicity of UnTHCPSi itself, as well as by the well-known biocompatibility features of HA. These

results demonstrated that both UnTHCPSi and UnTHCPSi–HA$^+$ can be, in general, safely utilized for drug delivery applications, considering the incubation times and the nanoparticle concentrations tested here.

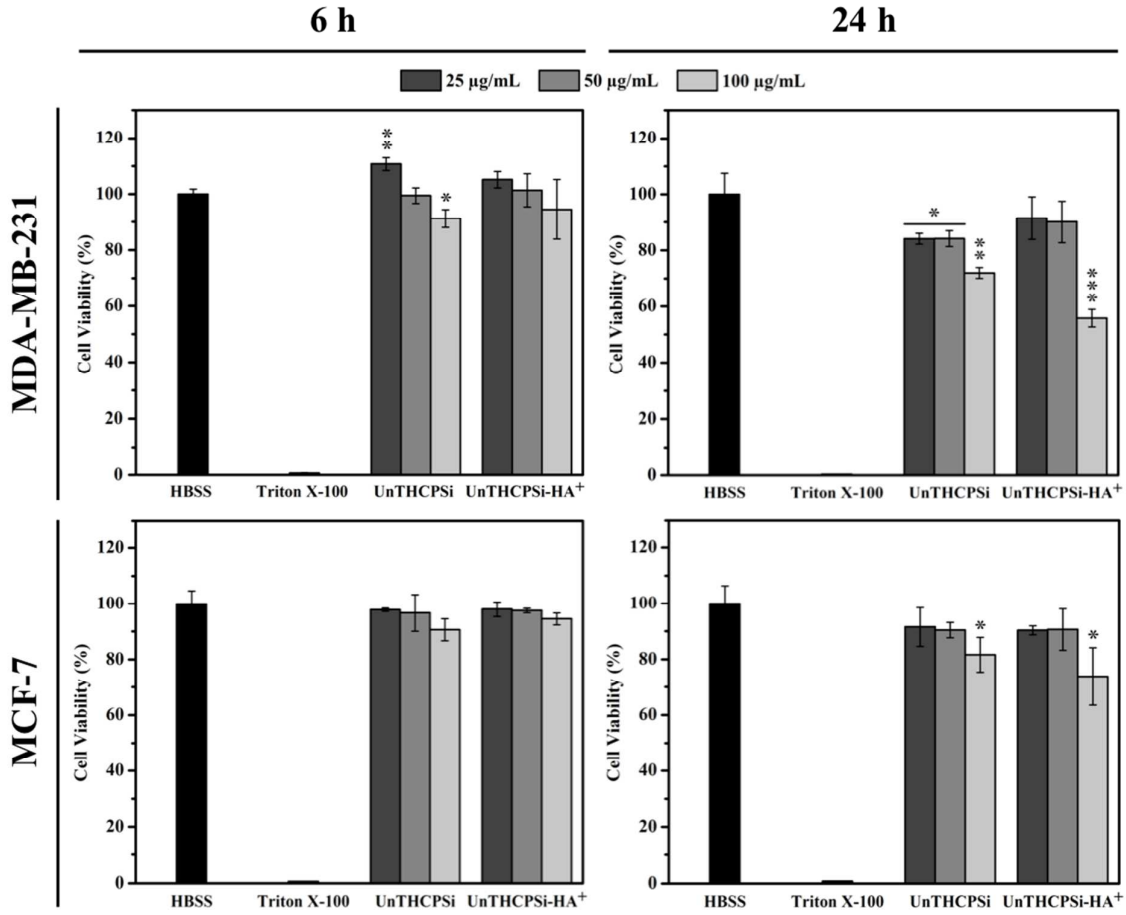

Figure 3. *In vitro* cytotoxicity of UnTHCPSi and UnTHCPSi–HA$^+$ nanoparticles, after incubation with MDA-MB-231 and MCF-7 breast cancer cell lines for 6 and 24 h at 37 ºC. The cell viability was evaluated by an ATP-based luminescent assay, after exposure of the cells to different concentrations of the nanoparticles. Cells cultured with HBSS (pH 7.4) and with 1% Triton X-100 were used as positive and negative controls, respectively. Error bars represent mean ± s.d. ($n \geq 3$). Statistical analysis was performed by means of the Student's *t*-test with the level of significance set at probabilities of *$p < 0.05$, **$p < 0.01$, and ***$p < 0.001$.

Cellular internalization of the nanoparticles

The efficient and targeted drug delivery, including the intracellular uptake, is also considered a prerequisite and, simultaneously, challenge in the development of nanomedicines for cancer therapy. [2] Although the size of the nanocarriers contributes significantly, not only to its passive accumulation in the tumor sites via the EPR effect, [7, 8] but also to its interaction with the cells, the surface chemical and biofunctional composition seems to play a key role in various essential properties, such as dispersibility, biocompatibility, and also cellular targeting and uptake. [18, 21, 29, 41]

In order to understand the behavior of the UnTHCPSi and UnTHCPSi–HA^+ nanoparticles at the cellular level, the cellular internalization and the intracellular distribution of both the nanoparticles were evaluated by TEM imaging (Figure 4). In this experiment, MDA-MB-231 and MCF-7 breast cancer cells were incubated with a concentration of 50 μg/mL of UnTHCPSi and UnTHCPSi–HA^+ nanoparticles for 6 h at 37 ºC.

The TEM images elucidated that the association and internalization of the bare UnTHCPSi nanoparticles with both cell lines was negligible, which can be possibly explained by the negative charge, as well as by the deficient colloidal stability of these nanoparticles. Contrarily, when functionalized with HA^+, and despite the less pronouncedly negative ζ-potential, the nanoparticles were massively associated with the cell membrane and further internalized by both MDA-MB-231 and MCF-7 cells, after which they seemed to be mainly enclosed in the endosomes of the cells. Although the aforementioned improved colloidal stability of UnTHCPSi–HA^+ nanoparticles favors their internalization by the cancer cells, the HA^+-mediated targeting of CD44 receptor might be a driven force for the enhanced interaction and internalization of the nanoparticles by the breast cancer cells. These results

represent a clear evidence of the enhanced cellular association of UnTHCPSi–HA$^+$ when compared with bare UnTHCPSi nanoparticles.

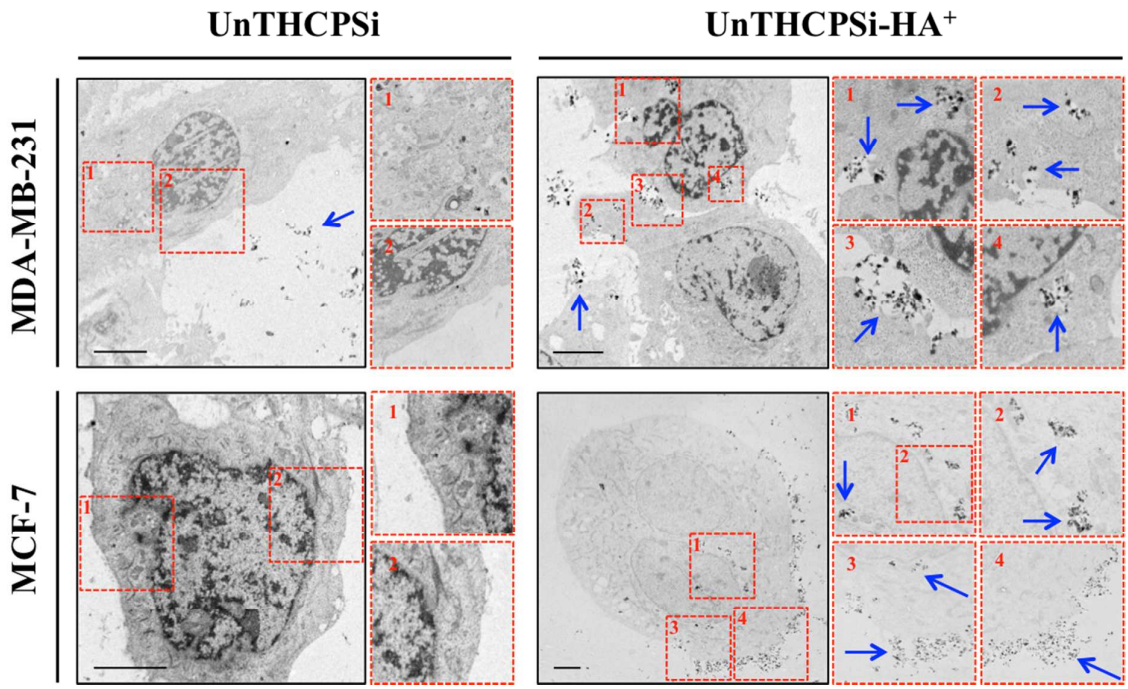

Figure 4. Intracellular uptake and distribution of the UnTHCPSi and UnTHCPSi–HA$^+$ nanoparticles. TEM images and correspondent numerically organized magnifications of ultra-thin sections of MDA-MB-231 and MCF-7 breast cancer cells exposed to UnTHCPSi and UnTHCPSi–HA$^+$ at a concentration of 50 μg/mL, for 6 h at 37 ºC. The conjugation of HA$^+$ onto the surface of the UnTHCPSi nanoparticles shown to significantly enhance the interaction and consequent uptake of the nanoparticles by both MDA-MB-231 and MCF-7 breast cancer cells. The nanoparticles associated with the cells are highlighted by the blue arrows. Scale bars are 5 μm.

Flow cytometric analysis of CD44 expression and cellular association

The expression of CD44 receptor in both MDA-MB-231 and MCF-7 breast cancer cells was evaluated by flow cytometry, after staining the cells with PE-CF594-labeled anti-human CD44 antibody (ESI S2†). When compared to the respective negative controls, both the cell

lines studied were shown to express the CD44 receptor, as elucidated by the increase on the mean fluorescence intensity of the stained cells. However, the incubation of MCF-7 cancer cells with up to 4-fold increased anti-human CD44 antibody concentration was not reflected on an intensification of the mean fluorescence intensity, which experienced an approximate 9-fold increase in comparison with unstained cells regardless of the antibody concentration, thus indicating the saturation of the receptors promptly available for interacting with the complementary antibody. Contrarily, in the case of MDA-MB-231 cancer cells, the successive increase in the anti-human CD44 antibody concentration resulted in a consecutive intensification of the fluorescence signal up to approximately 670-fold comparatively to the controls, suggesting significantly higher levels of CD44 expression in MDA-MB-231 than in MCF-7 breast cancer cells. [50]

In order to correlate the levels of CD44 expression with the cellular association of the UnTHCPSi and UnTHCPSi–HA^+ nanoparticles with MDA-MB-231 and MCF-7 breast cancer cells, both nanoparticles at the concentrations of 50 and 100 μg/mL were labeled with fluorescein isothiocyanate (FITC) prior to incubation with the cells for 6 h at 37 ºC and subsequent analysis by flow cytometry (Figure 5).

Regarding the incubation of the cells with the lower nanoparticle concentration of 50 μg/mL, no considerable variations were observed on the fluorescence peaks correspondent to the bare UnTHCPSi nanoparticles, when compared to the respective controls. In contrast, the fluorescent intensity of the cells incubated with UnTHCPSi–HA^+ was considerably higher than with bare UnTHCPSi, particularly in the case of MDA-MB-231. Furthermore, when incubated with bare UnTHCPSi nanoparticles at the concentration of 100 μg/mL, both cells exhibited similar trend on fluorescence intensity enhancement compared to the controls. Following the conjugation of HA^+ onto the surface of the UnTHCPSi nanoparticles, the fluorescence signal experienced a significant increase of 29.5 and 8.3-fold for MDA-MB-

231, as well as 4.9 and 1.8-fold for MCF-7 cells, compared to their negative controls and bare nanoparticle counterparts, respectively. However, contrarily to bare UnTHCPSi and in agreement with the results obtained for the lower nanoparticle concentration, the amplification in the fluorescence signal was extensively higher for MDA-MB-231.

Concerning the bare UnTHCPSi nanoparticles, a concentration dependent cellular association trend was observed, independently of the cell line studied. In contrast, in the case of UnTHCPSi–HA^+ and in agreement with the data obtained for the CD44 expression, the nanoparticles were found to interact with the cells in considerably higher extents when compared to the bare counterparts, particularly and more significantly in CD44-overexpressing MDA-MB-231 cancer cells, thereby suggesting that the enhancement in the cellular association and internalization is mediated by the efficient targeting of CD44 receptors via the conjugated HA^+, as depicted in Scheme 1B.

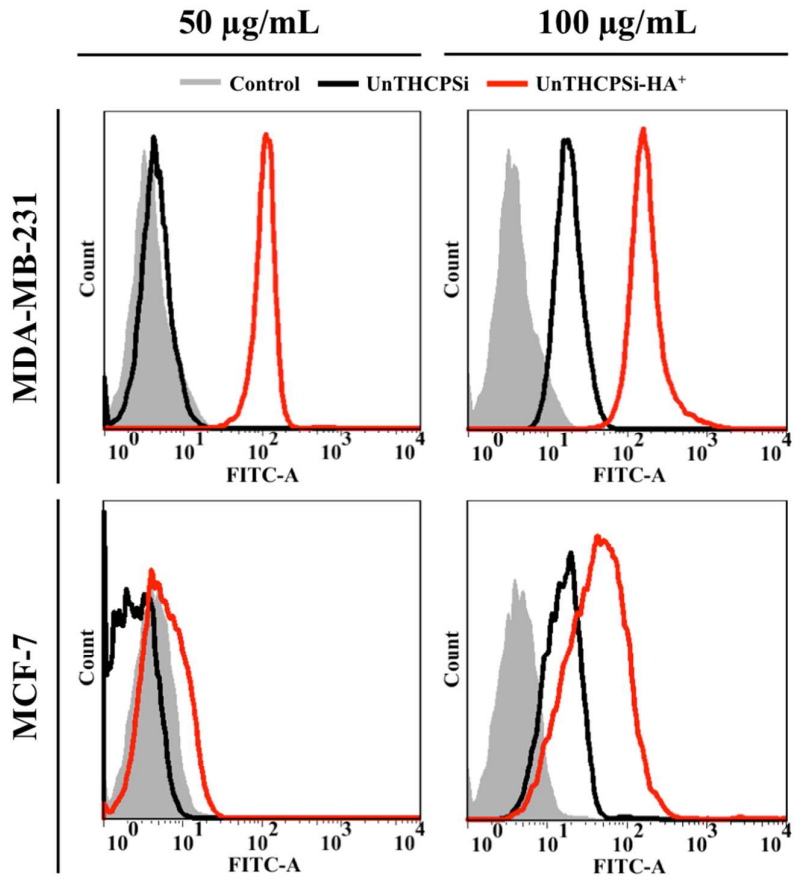

Figure 5. Flow cytometric analysis of the cellular association of UnTHCPSi and UnTHCPSi–HA^+ nanoparticles with MDA-MB-231 and MCF-7 breast cancer cells. The cells were incubated with UnTHCPSi and UnTHCPSi–HA^+ nanoparticles at the concentrations of 50 and 100 μg/mL for 6 h at 37 ºC. An enhanced association of the UnTHCPSi nanoparticles with both cell lines was observed after the biofunctionalization with HA^+.

Conclusions

We reported here the preparation of a PSi-based nanodelivery system that encompasses the attractive and promising physicochemical and biological properties of both HA and PSi materials, by covalently conjugating an amide-modified HA-derived polymer on the surface of the UnTHCPSi nanoparticles. The resulting UnTHCPSi–HA^+ was revealed not only to maintain some of the physicochemical key features of the PSi nanoparticles, such as relatively small size, reduced PdI, and high biocompatibility, but also showed improved colloidal and human plasma stability, and enhanced cellular interactions and internalization. The efficient targeting of CD44 receptor is highly dependent on its expression levels on the surface of the cells. Herein, we demonstrated that the enhanced cellular association of UnTHCPSi–HA^+ relies on the capability of the conjugated HA^+ to bind and consequently target the CD44-receptor overexpressing on the surface of the breast cancer cell lines. We hypothesize that, in a *in vivo* scenario, the developed nanocarrier will preferably accumulate in the CD44 overexpressing tumors in detriment of the non-malignant tissues with low CD44 expression levels, *via* HA^+-mediated targeting of the CD44-receptor. Overall, the nanodelivery system developed herein presents a suitable and promising nanoplatform for tumor drug delivery, particularly when aiming for the targeting of CD44 overexpressing cell tumors.

Acknowledgments

Patrick Almeida acknowledges the Finnish Cultural Foundation for a PhD scholarship (grant no. 00130129). Dr. Hélder A. Santos acknowledges financial support from the Academy of Finland (decision nos. 252215 and 256394), the University of Helsinki Funds, Biocentrum Helsinki, and the European Research Council under the European Union's Seventh Framework Programme (FP/2007–2013) grant no. 310892. Martti Kaasalainen acknowledges The National Doctoral Programme in Nanoscience (NGS-NANO).

Notes and references

1 *World Cancer Report 2014*, IARC, http://www.iarc.fr/en/publications/books/wcr/index.php, accessed April 2014.

2 R. K. Jain and T. Stylianopoulos, *Nat. Rev. Clin. Oncol.,* 2010, **7**, 653-664.

3 M. Mahmoudi, I. Lynch, M. R. Ejtehadi, M. P. Monopoli, F. B. Bombelli and S. Laurent, *Chem. Rev.,* 2011, **111**, 5610-5637.

4 P. P. Karmali and D. Simberg, *Expert Opin. Drug Deliv.,* 2011, **8**, 343-357.

5 I. Lynch, A. Salvati and K. A. Dawson, *Nat. Nanotechnol.,* 2009, **4**, 546-547.

6 T. Cedervall, I. Lynch, S. Lindman, T. Berggård, E. Thulin, H. Nilsson, K. A. Dawson and S. Linse, *Proc. Natl. Acad. Sci. U. S. A.,* 2007, **104**, 2050-2055.

7 J. Fang, H. Nakamura and H. Maeda, *Adv. Drug Deliv. Rev.,* 2011, **63**, 136-151.

8 H. Maeda, *The enhanced permeability and retention (EPR) effect in tumor vasculature: The key role of tumor-selective macromolecular drug targeting*, *Adv. Enzyme Regul.*, 2001, **41**, 189-207.

9 H. L. Zhao, C. Xue, J. L. Du, M. Ren, S. Xia, Y. G. Cheng and Z. M. Liu, *J. Control. Release,* 2012, **159**, 346-352.

10 A. K. Varkouhi, M. Scholte, G. Storm and H. J. Haisma, *J. Control. Release,* 2011, **151**, 220-228.

11 H. A. Santos, L. M. Bimbo, V.-P. Lehto, A. J. Airaksinen, J. Salonen and J. Hirvonen, *Curr. Drug Discov. Tech.*, 2011, **8**, 228-249.

12 J. Salonen, A. M. Kaukonen, J. Hirvonen and V. -. Lehto, *J. Pharm. Sci.,* 2008, **97**, 632-653.

13 P. Kinnari, E. Mäkilä, T. Heikkilä, J. Salonen, J. Hirvonen and H. A. Santos, *Int. J. Pharm.,* 2011, **414**, 148-156.

14 R. E. Serda, B. Godin, E. Blanco, C. Chiappini and M. Ferrari, *Biochim. Biophys. Acta,* 2011, **1810**, 317-329.

15 E. Tasciotti, X. Liu, R. Bhavane, K. Plant, A. D. Leonard, B. K. Price, M. M. Cheng, P. Decuzzi, J. M. Tour, F. Robertson and M. Ferrari, *Nat. Nanotechnol.*, 2008, **3**, 151-157.

16 H. A. Santos, L. M. Bimbo, B. Herranz, M.-A. Shahbazi, J. Hirvonen and J. Salonen, *J. Mater. Res.,* 2013, **28**, 152-164.

17 C. Chiappini, E. Tasciotti, J. R. Fakhoury, D. Fine, L. Pullan, Y. Wang, L. Fu, X. Liu and M. Ferrari, *ChemPhysChem,* 2010, **11**, 1029-1035.

18 L. M. Bimbo, M. Sarparanta, H. A. Santos, A. J. Airaksinen, E. Mäkilä, T. Laaksonen, L. Peltonen, V.-P. Lehto, J. Hirvonen and J. Salonen, *ACS Nano,* 2010, **4**, 3023-3032.

19 L. M. Bimbo, E. Mäkilä, T. Laaksonen, V.-P. Lehto, J. Salonen, J. Hirvonen and H. A. Santos, *Biomaterials,* 2011, **32**, 2625-2633.

20 D. Liu, L. M. Bimbo, E. Mäkilä, F. Villanova, M. Kaasalainen, B. Herranz-Blanco, C. M. Caramella, V.-P. Lehto, J. Salonen, K. -. Herzig, J. Hirvonen and H. A. Santos, *J. Control. Release,* 2013, **170**, 268-278.

21 C. Wang, E. M. Mäkilä, M. H. Kaasalainen, D. Liu, M. P. Sarparanta, A. J. Airaksinen, J. J. Salonen, J. T. Hirvonen and H. A. Santos, *Biomaterials,* 2014, **35**, 1257-1266.

22 D. Liu, H. Zhang, B. Herranz-Blanco, E. Mäkilä, V. Lehto, J. Salonen, J. Hirvonen and H. A. Santos, *Small,* 2014, **10**, 2029-2038.

23 B. Herranz-Blanco, L. R. Arriaga, E. Mäkilä, A. Correia, N. Shrestha, S. Mirza, D. A. Weitz, J. Salonen, J. Hirvonen and H. A. Santos, *Lab Chip*, 2014, **14**, 1083-1086.

24 M. Kilpeläinen, J. Mönkäre, M. A. Vlasova, J. Riikonen, V.-P. Lehto, J. Salonen, K. Järvinen and K.-H. Herzig, *Eur. J. Pharm. Biopharm.,* 2011, **77**, 20-25.

25 M. Kovalainen, J. Mönkäre, E. Mäkilä, J. Salonen, V.-P. Lehto, K.-H. Herzig and K. Järvinen, *Pharm. Res.,* 2012, **29**, 837-846.

26 M. Kovalainen, J. Mönkäre, M. Kaasalainen, J. Riikonen, V. -. Lehto, J. Salonen, K.-H. Herzig and K. Järvinen, *Mol. Pharmaceutics,* 2013, **10**, 353-359.

27 T. Tanaka, L. S. Mangala, P. E. Vivas-Mejia, R. Nieves-Alicea, A. P. Mann, E. Mora, H. Han, M. M. K. Shahzad, X. Liu, R. Bhavane, J. Gu, J. R. Fakhoury, C. Chiappini, C. Lu, K. Matsuo, B. Godin, R. L. Stone, A. M. Nick, G. Lopez-Berestein, A. K. Sood and M. Ferrari, *Cancer Res.,* 2010, **70**, 3687-3696.

28 N. Hasan, A. Mann, M. Ferrari and T. Tanaka, *Methods Mol. Biol.,* 2013, **1049**, 481-493.

29 M.-A. Shahbazi, M. Hamidi, E. M. Mäkilä, H. Zhang, P. V. Almeida, M. Kaasalainen, J. J. Salonen, J. T. Hirvonen and H. A. Santos, *Biomaterials,* 2013, **34**, 7776-7789.

30 S. P. Low, N. H. Voelcker, L. T. Canham and K. A. Williams, *Biomaterials,* 2009, **30**, 2873-2880.

31 T. Tanaka, B. Godin, R. Bhavane, R. Nieves-Alicea, J. Gu, X. Liu, C. Chiappini, J. R. Fakhoury, S. Amra, A. Ewing, Q. Li, I. J. Fidler and M. Ferrari, *Int. J. Pharm.,* 2010, **402**, 190-197.

32 M. Kilpeläinen, J. Riikonen, M. A. Vlasova, A. Huotari, V.-P. Lehto, J. Salonen, K.-H. Herzig and K. Järvinen, *J. Control. Release,* 2009, **137**, 166-170.

33 K. L. Jarvis, T. J. Barnes and C. A. Prestidge, *Adv. Colloid Interface Sci.,* 2012, **175**, 25-38.

34 E. C. Wu, J. S. Andrew, L. Cheng, W. R. Freeman, L. Pearson and M. J. Sailor, *Biomaterials,* 2011, **32**, 1957-1966.

35 M.-A. Shahbazi, P. V. Almeida, E. Mäkilä, A. Correia, M. P. A. Ferreira, M. Kaasalainen, J. Salonen, J. Hirvonen and H. A. Santos, *Macromol. Rapid Commun.,* 2014, 2014, **35**, 624-629.

36 B. Guan, S. Ciampi, G. Le Saux, K. Gaus, P. J. Reece and J. J. Gooding, *Langmuir,* 2011, **27**, 328-334.

37 M. Sarparanta, L. M. Bimbo, J. Rytkoänen, E. Mäkilä, T. J. Laaksonen, P. Laaksonen, M. Nyman, J. Salonen, M. B. Linder, J. Hirvonen, H. A. Santos and A. J. Airaksinen, *Mol. Pharmaceutics,* 2012, **9**, 654-663.

38 L. M. Bimbo, E. Mäkilä, J. Raula, T. Laaksonen, P. Laaksonen, K. Strommer, E. I. Kauppinen, J. Salonen, M. B. Linder, J. Hirvonen and H. A. Santos, *Biomaterials,* 2011, **32**, 9089-9099.

39 L. M. Bimbo, M. Sarparanta, E. Mäkilä, T. Laaksonen, P. Laaksonen, J. Salonen, M. B. Linder, J. Hirvonen, A. J. Airaksinen and H. A. Santos, *Nanoscale,* 2012, **4**, 3184-3192.

40 M. P. Sarparanta, L. M. Bimbo, E. M. Mäkilä, J. J. Salonen, P. H. Laaksonen, A. M. K. Helariutta, M. B. Linder, J. T. Hirvonen, T. J. Laaksonen, H. A. Santos and A. J. Airaksinen, *Biomaterials,* 2012, **33**, 3353-3362.

41 P. J. Kinnari, M. L. K. Hyvönen, E. M. Mäkilä, M. H. Kaasalainen, A. Rivinoja, J. J. Salonen, J. T. Hirvonen, P. M. Laakkonen and H. A. Santos, *Biomaterials,* 2013, **34**, 9134-9141.

42 C.-F. Wang, E. M. Mäkilä, M. H. Kaasalainen, D. Liu, M. P. Sarparanta, A. J. Airaksinen, J. J. Salonen, J. T. Hirvonen and H. A. Santos, *Biomaterials,* 2014, **35**, 1257-1266.

43 B. P. Toole, *Nat. Rev. Cancer,* 2004, **4**, 528-539.

44 K. S. Girish and K. Kemparaju, *Life Sci.,* 2007, **80**, 1921-1943.

45 S. Goodison, V. Urquidi and D. Tarin, *J Clin. Pathol.*, 1999, **52**, 189-196.

46 J. Lesley, R. Hyman, N. English, J. B. Catterall and G. A. Turner, *Glycoconj. J.,* 1997, **14**, 611-622.

47 A. Aruffo, I. Stamenkovic, M. Melnick, C. B. Underhill and B. Seed, *Cell,* 1990, **61**, 1303-1313.

48 J. Entwistle, C. L. Hall and E. A. Turley, *J. Cell. Biochem.,* 1996, **61**, 569-577.

49 H. Ponta, L. Sherman and P. A. Herrlich, *Nat. Rev. Mol. Cell Biol.*, 2003, **4**, 33-45.

50 M. Veiseh and E. A. Turley, *Integr. Biol.*, 2011, **3**, 304-315.

51 M. Birch, S. Mitchell and I. R. Hart, *Cancer Res.,* 1991, **51**, 6660-6667.

52 M. S. Sy, Y. -. Guo and I. Stamenkovic, *J. Exp. Med.,* 1991, **174**, 859-866.

53 D. A. Ossipov, *Expert Opin. Drug Deliv.*, 2010, **7**, 681-703.

54 Y. Huh, H.-J. Cho, I.-S. Yoon, M.-K. Choi, J. S. Kim, E. Oh, S.-J. Chung, C.-K. Shim, D.-D. Kim, *Eur J. Pharm. Sci.*, 2010, **40**, 9-15.

55 A. Schneider, C. Picart, B. Senger, P. Schaaf, J. Voegel and B. Frisch, *Langmuir,* 2007, **23**, 2655-2662.

56 S. Brunauer, P. H. Emmett and E. Teller, *J. Am. Chem. Soc.,* 1938, **60**, 309-319.

57 K. S. W. Sing, *Pure Appl. Chem.*, 1985, **56**, 603-619.

58 K. Haxaire, Y. Maréchal, M. Milas and M. Rinaudo, *Biopolymers,* 2003, **72**, 10-20.

59 G. Liut and K. Cui, *Carbohydr. Res.,* 1996, **285**, 167-172.

60 J.-H. Park, L. Gu, G. Von Maltzahn, E. Ruoslahti, S. N. Bhatia and M. J. Sailor, *Nat. Mater.*, 2009, **8**, 331-336.

61 L.-S. Wang, L.-C. Wu, S.-Y. Lu, L.-L. Chang, I.-T. Teng,. C.-M. Yang and J.-A. A. Ho, *ACS Nano,* 2010, **4**, 4371-4379.

62 Z. Dong, W. Zheng, Z. Xu and Z. Yin, *J. Appl. Polym. Sci.,* 2013, **130**, 927-932.

63 K. K. Upadhyay, A. N. Bhatt, E. Castro, A. K. Mishra, K. Chuttani, B. S. Dwarakanath, C. Schatz, J.-F. Le Meins, A. Misra and S. Lecommandoux, *Macromol. Biosci.*, 2010, **10**, 503-512.

64 K. K. Upadhyay, A. K. Mishra, K. Chuttani, A. Kaul, C. Schatz, J. -. Le Meins, A. Misra and S. Lecommandoux, *Nanomedicine*, 2012, **8,** 71-80.

65 D. Peer and R. Margalit, *Neoplasia,* 2004, **6**, 343-353.

66 S. Bhattacharjee, D. Ershov, K. Fytianos, J. van der Gucht, G. M. Alink, I. M. C. M. Rietjens, A. T. M. Marcelis and H. Zuilhof, *Part. Fibre Toxicol.*, 2012, **9**, 11.